Design and analysis for an asymmetric LMA-PCF with low bending loss and effective single-mode operation

M. WANG, H. YANG*, P. JIANG, W. CAIYANG, Y. QIN, M. ZHOU
School of Physics, University of Electronic Science and Technology of China, Chengdu 610054, China

A novel structure of large-mode-area photonic crystal fiber (LMA-PCF) with elliptical air hole is proposed and investigated in this paper. The design of the novel photonic crystal fiber works on the principle of bend-induced mode filtering. On this basis, the idea of using the new parameters of the eccentricity of the ellipse to control the bending losses of the fundamental and first higher order modes was proposed. The fiber structure proposed in this paper has the potential to be applied to compact high-power delivery devices, which is of great significance for high-power laser systems and optical amplifiers.

1. Introduction

In the past few decades, high-power fiber lasers have developed very rapidly. This type of fiber laser has many excellent features, including excellent beam quality, good heat dissipation, compact size, and low operating costs [1-5]. However, as the output power increases further, the nonlinear effects of the fiber become a key factor limiting power increase. In order to solve this problem and suppress optical nonlinear effects, we need to find ways to increase the mode area of the fiber. By increasing the core size, we can get a larger mode area (LMA), which may damage the high-power beam quality because of the mode instability phenomenon [6-8]. In order to avoid the instability of the mode, the fiber needs to maintain effective single mode operation while achieving the goal of obtaining a large mode area. Different methods have been reported in the literature, which can help us suppress high-order modes (HOMs) from the fiber structure of the large mode area while maintaining single-mode (SM) operation [9,10].

The performance of traditional fiber often fails to meet our expectations. For example, if a step-index fiber with the effective mode area (EMA) of no more than 450 μm^2 wants to maintain single-mode operation at the wavelength of 1.064 μm, its numerical aperture (NA) must be less than 0.027. In the above case, a large bending loss is generated, and the bending loss of the step-index fiber reaches 3.3 dB/m when the bending radius is 50 cm [11]. However, as time goes on, new fiber designs will continue to emerge and these fibers will exhibit even better performance.

Several efforts have been made for the sake of LMA fiber with low bending loss. In 2016, Saini et al. reported an asymmetric design of solid core LMA PCF with a mode area of 1530 μm^2 and bending loss of 0.25 dB/m with a bending radius of 30 cm [12]. In order to achieve a larger mode area, some holes of the solid core LMA PCF have been modified by introducing fluorine-doped fused silica rods. Obviously, this fiber achieves a larger mode area, but the fabrication process is more complicated. Moreover, when the bending radius reaches 15 cm, the

bending loss of the fundamental mode is greater than 10 dB/m, so this structure is not suitable for a smaller bending radius.

In 2018, Y.QIN *et al.* reported a novel PCF structure. According to their research, the effective mode area of the fundamental mode is 1005 μm² under the bending radius of only 10 cm at the wavelength of 1.55 μm. Under the same condition, the bending loss of the fundamental mode is 0.0113 dB/m [13]. In 2018, S. Ma *et al.* reported a novel design of segmented cladding fiber (SCF) with resonant ring. According to their research, the

effectively single-mode operation with a mode area of 790 μm² can be achieved at a bend radius of 15 cm [14]. At almost the same time, a novel structure of modified multi-trench fiber (MTF) was proposed. The loss ratio of this MTF between lowest-HOM and fundamental mode (FM) is more than 300 with the mode area of 840 μm² under bending radius of 15 cm [15]. For a more convenient digital comparison, we have included some of the performance parameters of the different fibers mentioned above in Table 1.

Table 1. Detailed comparisons of A_{eff} and losses between different fibers with large mode area and single-mode operation

Fibers	λ (nm)	R(cm)	A_{eff}(μm²)	**Bending loss**(dB/m)
Fluorine-doped PCF [12]	1064	30	1530	0.25
Hybrid cladding PCF [13]	1550	10	1005	0.0113
SCF [14]	1064	15	790	0.015
MTF [15]	1064	15	840	<0.05

In this paper, a novel structure of LMA-PCF with large mode area and effective single-mode operation by introducing elliptical air holes is proposed. The design of the novel photonic crystal fiber works on the principle of bend-induced mode filtering. These circular air holes and elliptical air holes control the mode field inside the core region. The single-mode operation is ensured by introducing low bend loss for the fundamental mode and high bend loss for the first higher order. Numerical results show that this structure can achieve large mode area and effective single-mode operation with low bend loss for the fundamental mode at the wavelength of 1.064 μm. The effective mode area of the fundamental mode is 1228 μm² when the bending radius is 15 cm. The bending loss of the fundamental mode is just 9.0038×10^{-4} dB/m, and the loss ratio between the fundamental and high-order modes of the bending loss is larger than 1200 when the bending radius is 15 cm.

2. Design of LMA-PCF

Due to the immature production process, minor errors are inevitable when preparing photonic crystal fibers. For example, some theoretically should be

processed into circular air holes, which will eventually produce tiny shape distortions. Perfecting the photonic crystal fiber preparation process and eliminating errors have become the first choice. We have also been thinking about the effects of distortion in the shape of these air holes on the performance of the fiber. After that, we discovered that the distortion of the air holes may bring better performance to the photonic crystal fiber.
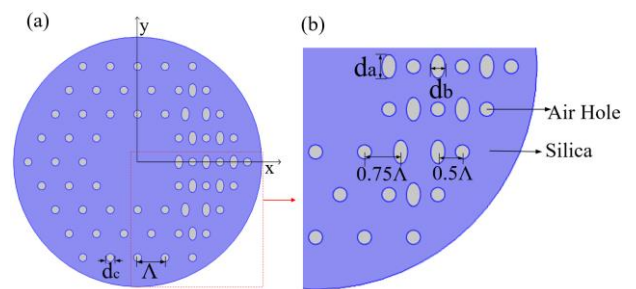
Fig. 1. The transverse cross-sectional view of proposed LMA PCF structure (color online)

The effects of distortion of various fiber structures on fiber performance are investigated. Based on this, a new type of asymmetric structure photonic crystal fiber is proposed. The transverse cross-sectional view of

proposed LMA PCF structure is depicted in Fig. 1. As shown in Fig. 1(a), the x-axis is the axis of symmetry of the fiber cross section, but the y-axis is not. And Fig. 1(b) is an enlarged view of the lower right corner of Fig. 1(a). As shown in the figure, the idea of the design is derived from a conventional triangular lattice structure photonic crystal fiber. The original model was that some of the air holes were arranged in a hexagonal lattice in silica dielectric, and we made some changes in this model. To construct a larger core, we removed nine circular air holes in the base fiber structure. In addition, in order to achieve lower fundamental mode losses in curved fibers while providing leakage channels for higher order modes, we added thirteen elliptical air holes to the right side of the fiber structure. The pitch of the circular air holes is Λ. In Fig. 1(b), the distance between only one elliptical air hole and the laterally adjacent circular air hole is 0.75Λ, which has been marked in the figure. The distance between the remaining elliptical air holes in Fig. 1(b) and the laterally adjacent circular air holes is 0.5Λ. As shown in Fig. 1, in the proposed structure, the diameter of the circular air hole shown by d_c and the diameters of the elliptical air holes shown by d_b and d_a.

The Sellmeier equation is used to model the background material (silica) [16]:

$$n^2(\lambda) = 1 + \frac{B_1\lambda^2}{\lambda^2 - C_1} + \frac{B_2\lambda^2}{\lambda^2 - C_2} + \frac{B_3\lambda^2}{\lambda^2 - C_3} \qquad (1)$$

In Eq. (1), n is the refractive index of silica and λ is the wavelength in μm. The values of the coefficients are defined as follows: B_1=0.69616300, B_2=0.407942600, B_3=0.897479400, C_1=4.67914826×10⁻³ μm², C_2=1.35120631×10⁻² μm², C_3= 97.9340025 μm². As a result, the refractive index of the background material is n_0=1.45 at a wavelength of 1.064μm.

3. Method of analysis

The finite element method (FEM) is a highly efficient and commonly used numerical calculation method suitable for complex fiber structures. The fiber we proposed needs to work under bending conditions,

and the background material of the fiber will have different refractive indices under such conditions. Therefore, in this article we used the commercially available software COMSOL Multiphysics, which uses the finite element method and combines the boundary conditions of the perfect matching layer. A 25-μm-thick circular PML is set outside the pure silica layer. In the finite element scheme, we solve the following Maxwell vector equation [17,18] :

$$\nabla' \times \overrightarrow{H} = j\omega\varepsilon_0 n^2 s\overrightarrow{E} \qquad (2)$$

$$\nabla' \times \overrightarrow{E} = -j\omega\mu_0 s\overrightarrow{H} \qquad (3)$$

In Eq. (2) and Eq. (3), E is the electric field and H is the magnetic field. Furthermore, s is the PML parameter which is set as 1 outside the PML region, ε_0 and μ_0 are permittivity and permeability of vacuum, n is the refractive index, and ω is the angular frequency. The PML parameter s in the PML region is estimated as:

$$s = 1 - jk(\frac{\rho}{d})^2 \qquad (4)$$

$$k = \frac{3\lambda}{4\pi nd}\ln(\frac{1}{\exp(-\frac{2\sigma_{max}d}{3\varepsilon_0 cn})}) \qquad (5)$$

where ρ is the distance from the beginning of PML and d is the thickness of PML, λ is the operation wavelength, and σ_{max} is the maximum conductivity. When we solve the above equation for such bent PCF structures, the propagation constants of the modes become complex. Through the propagation constant, we can get the effective indices of the modes and the bend losses of the modes.

In this paper, the method of equivalent refractive index profile is used to express the bent PCF with an equivalent straight PCF whose refractive index profile n_{eq} is [19]:

$$n_{eq}(x, y) = n(x, y)(1 + \frac{x\cos\theta + y\sin\theta}{R}) \qquad (6)$$

where θ is the bending direction angle, R represents the bending radius and n(x, y) is the refractive index profile of straight LMA-PCE. In this paper, the bend direction is along the x axis and the default value of the bending direction angle is 0. In order to get more accurate results, we have adopted another equation [20]:

$$n_{eq} = n(x, y)\exp(\frac{x}{R}) \qquad (7)$$

The mode area and leakage loss of the fiber can be expressed as [21,22] :

$$A_{\text{eff}} = \frac{(\iint|E|^2 \mathrm{d}x\mathrm{d}y)^2}{(\int|E|^4 \mathrm{d}x\mathrm{d}y)} \qquad (8)$$

$$L(\frac{\mathrm{dB}}{\mathrm{m}}) = \frac{40\pi}{\ln(10)\lambda}\mathrm{Im}(n_{\text{eff}}) \qquad (9)$$

where E denotes the electric field, Im(n_{eff}) is the imaginary part of the effective refractive index, λ is the wavelength and is set as 1.064 μm in this paper. We set the loss of FM less than 0.1 dB/m and HOMs more than 1 dB/m as the baseline for effective SM operation [9].

$$e = \frac{\sqrt{d_{\mathrm{a}}^2 - d_{\mathrm{b}}^2}}{d_{\mathrm{a}}} \qquad (10)$$

In Eq. (10), e represents the eccentricity of the ellipse. When e is equal to 0, the elliptical air hole is a standard circular air hole.

4. Results and discussions

First, we set the initial values of the various parameters of the elliptical air hole LMA PCF proposed in this paper. We have chosen the values of the parameters as d_{a}=10 μm, d_{b}=6 μm, d_{c}=6 μm, Λ=21 μm, and R→∞. These initial values are gradually optimized in combination with the simulation results. Fig. 2 shows the

modal field distributions of different modes when the fiber is not bent. (a), (b), (c), and (d) in Fig. 2 respectively show the modal field distributions of LP_{01} mode, LP_{11v} mode, LP_{11h} mode, and LP_{21} mode [23-25].
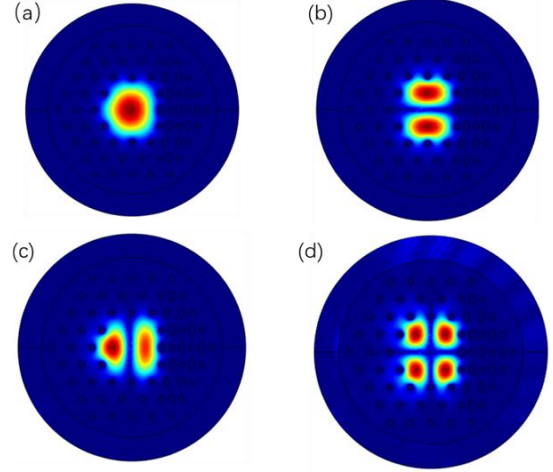
Fig. 2. (a), (b), (c), and (d) in Fig. 2 respectively show the modal field distributions of LP_{01} mode, LP_{11v} mode, LP_{11h} mode, and LP_{21} mode, when d_a=10 μm, d_b=6 μm, d_c=6 μm, Λ=21 μm, and R tends to ∞ (color online)

Fig. 2 indicates that, due to the asymmetric fiber design, the asymmetric mode field distribution will also appear in the straight fiber. Asymmetric fiber designs have more selectivity in implementing bend-induced mode filtering than symmetric fiber designs. However, as the bending radius is reduced, the bending loss of the fundamental mode is gradually increased. How to reduce the bending loss of the fundamental mode while ensuring the filtering of the high-order mode, which puts higher requirements on the design of our PCF. In this paper, we choose the mode with the lowest leakage loss from LP_{11v} mode and LP_{11h} mode as LP_{11} mode.

Fig. 3 illustrates the surface profile of the transverse electric field component in different modes and different bending radii when d_a=10 μm, d_b=6 μm, d_c=6 μm, Λ=21 μm. Fig. 3 indicates that, the fundamental mode can be well confined to the center of the fiber regardless of the bend radius. In contrast, as the bending radius decreases, the losses in the LP_{11} mode and the LP_{21} mode become larger, and even a large amount leaks into the cladding region of the fiber. This phenomenon indicates that the fiber proposed in this paper can effectively achieve mode

stripping. This mode stripping also provides a theoretical basis for the single-mode LMA-PCF.
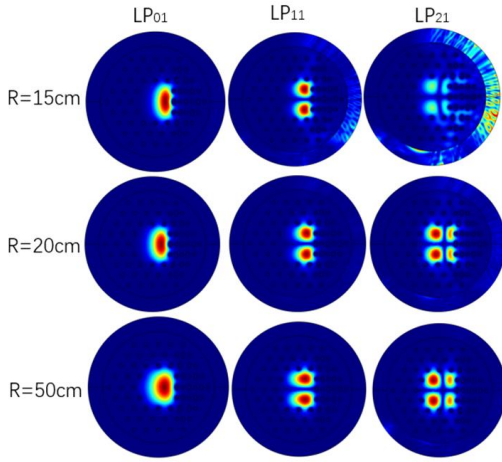
Fig. 3. Surface profile of the transverse electric field component in different modes and different bending radii when d_a=10 μm, d_b=6 μm, d_c=6 μm, Λ=21 μm (color online)
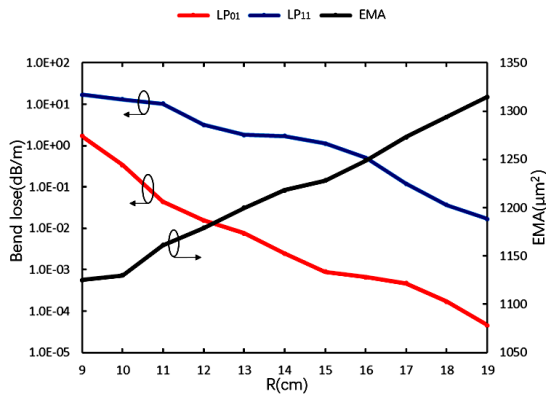
Fig. 4. Variation of the bend losses of LP_{01} and LP_{11} modes, and the effective mode area of the LP_{01} mode on the bending radius at 1.064 μm wavelength, when d_a=10 μm, d_b=6 μm, d_c=6 μm, Λ=21 μm (color online)

Fig. 4 illustrates the variation of the EMA of the LP_{01} mode and bend losses of LP_{01} and LP_{11} modes of the proposed structure with the parameter *R*. It indicates that the bend radius of the fiber has a significant impact on the performance of the fiber. The EMA of LP_{01} mode increases as the bending radius increases. In contrast, the bending losses of LP_{01} and LP_{11} modes decrease as the bending radius increases. Because the bending of the fiber causes a regular change in the refractive index of

the material inside the fiber, different bending radii correspond to different bending losses. According to Eq. (7), in the cladding region where x is greater than 0, the equivalent refractive index of the optical fiber decreases as R increases, so the limiting ability of the optical fiber cladding will be enhanced. Therefore, the bending loss decreases as the bending radius increases. In Fig. 4, when the bending radius is 15 cm, the bending loss of LP_{01} is 9.0038×10^{-4} dB/m, the bending loss of LP_{11} is 1.13 dB/m, and the EMA of the fundamental mode is 1228 μm². When the bending radius is less than 15 cm, the bending loss of the LP_{11} mode is larger than 1 dB/m, and when the bending radius is larger than 11 cm, the bending loss of the LP_{01} mode is less than 0.1 dB/m. Therefore, when the bending radius of the PCF proposed in Fig. 4 is between 11 cm and 15 cm, the PCF can achieve effective single-mode operation.
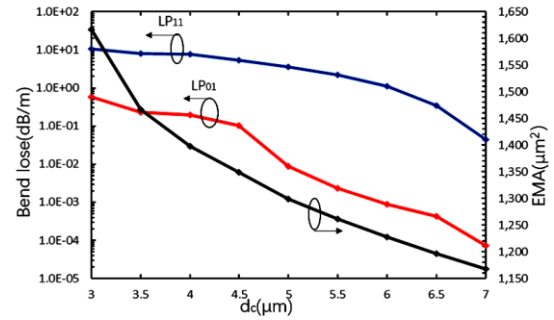
Fig. 5. Variation of the bend losses of LP_{01} and LP_{11} modes, and the effective mode area of the LP_{01} mode on d_c at 1.064 μm wavelength, when d_a=10 μm, d_b=6 μm, Λ=21 μm, and R=15 cm (color online)

Fig. 5 illustrates the variation of the EMA of the LP_{01} mode and bend losses of LP_{01} and LP_{11} modes of the proposed structure with the parameter d_c. The EMA of the LP_{01} mode decreases with d_c and the bend losses of first two modes also decrease on increasing the value of d_c. This phenomenon is due to the index contrast between the core and the cladding, which is related to the value of d_c. When the diameter of the circular air hole becomes larger, the area of the cladding area of the optical fiber becomes larger and the core area becomes smaller. The fundamental mode is confined in the core, so the effective mode area of the fundamental mode will

become smaller due to the larger diameter of the circular air hole.
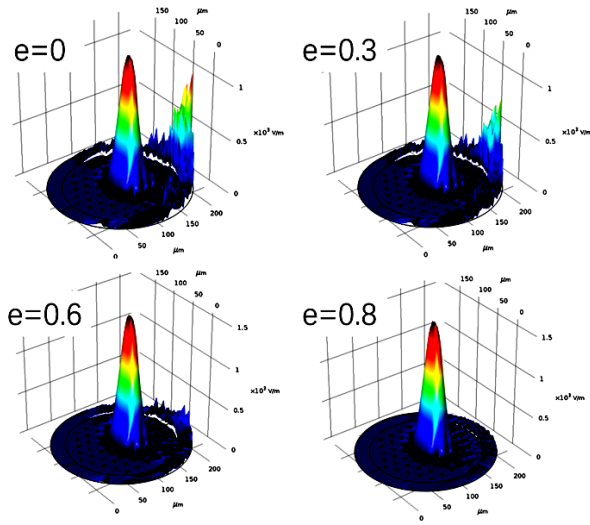
Fig. 6. The corresponding mode field distribution of FM is obtained when the eccentricity is 0, 0.3, 0.6, and 0.8, with d_b=6 μm, d_c=6 μm, Λ=21 μm, and R=15 cm (color online)

Fig. 6 depicts the corresponding mode field distribution of FM for eccentricities of 0, 0.3, 0.6, and 0.8. From Fig. 6, we can see that as the eccentricity increases, the peak on the right side of the fiber becomes lower and lower. The peak on the right side of the fiber is the part of the fundamental mode leakage. Therefore, as the eccentricity increases, the bending loss of the fundamental mode becomes smaller and smaller.
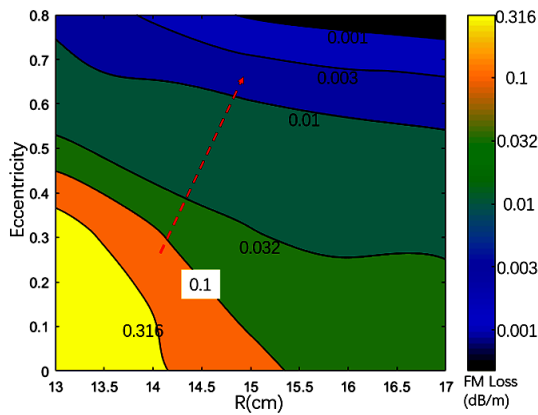
Fig. 7. Joint effects of eccentricity and bending radius on loss of FM with d_b=6 μm, d_c=6 μm, Λ=21 μm (color online)
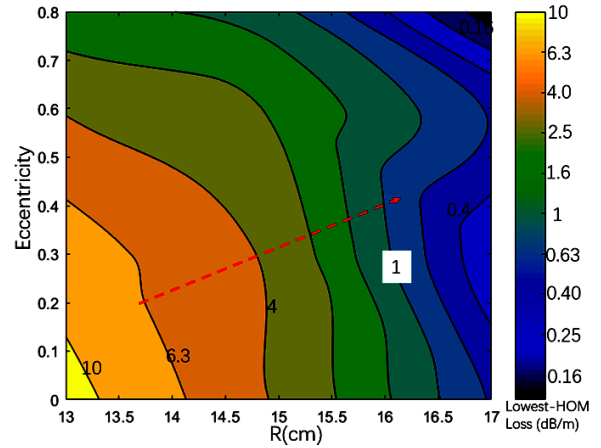
Fig. 8. Joint effects of eccentricity and bending radius on loss of lowest-HOMs with d_b=6 μm, d_c=6 μm, Λ=21 μm (color online)
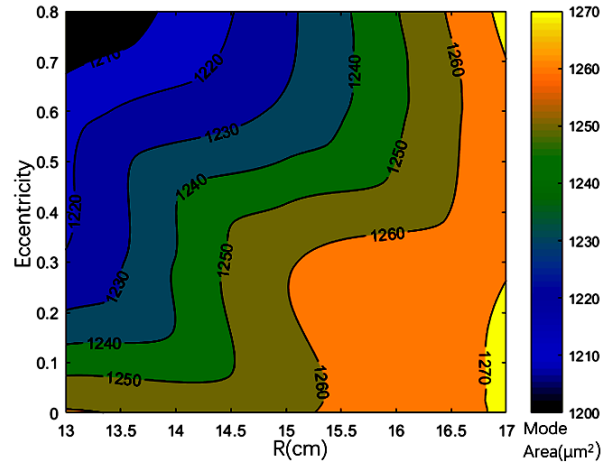
Fig. 9. Joint effects of eccentricity and bending radius on EMA with d_b=6 μm, d_c=6 μm, Λ=21 μm (color online)

Fig. 7 depicts the joint effects of eccentricity and bending radius on loss of FM with d_b=6 μm, d_c=6 μm, Λ=21 μm. The red arrow in Fig. 7 indicates the main direction of the reduction in bending loss of FM. Fig. 8 depicts the joint effects of eccentricity and bending radius on loss of lowest-HOMs with d_b=6 μm, d_c=6 μm, Λ=21 μm. The red arrow in Fig. 8 indicates the main direction of the reduction in bending loss of lowest-HOMs. Fig. 9 depicts the joint effects of eccentricity and bending radius on EMA. By comparing the directions indicated by the red arrows in Figs. 7 and 8, we can conclude that the eccentricity has a more positive effect on the fundamental mode than the higher order

modes. Therefore, we can more effectively separate the fundamental mode and the higher order mode by adjusting the values of the eccentricity and the bending radius.
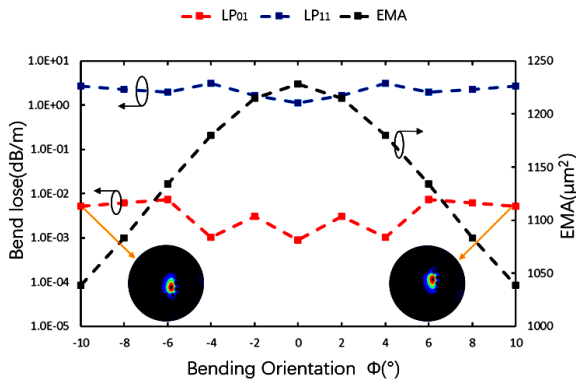
Fig. 10. Variation of the bend losses of LP$_{01}$ and LP$_{11}$ modes, and the effective mode area of the LP$_{01}$ mode on bending orientation at 1.064 μm wavelength, when d$_a$=10 μm, d$_b$=6 μm, d$_c$=6 μm, Λ=21 μm, and R=15 cm (color online)

Fig. 10 illustrates the variation of the bend losses of LP$_{01}$ and LP$_{11}$ modes, and the effective mode area of the LP$_{01}$ mode on bending orientation at 1.064 μm wavelength, when d_a=10 μm, d_b=6 μm, d_c=6 μm, $Λ$=21 μm, and R=15 cm. As can be seen from Fig. 10, as the bending orientation changes, the EMA of the fundamental mode changes significantly. When a deviation of about 10° is generated, it is still possible to ensure that the EMA of the FM is > 1000 μm^2, effective single-mode operation, and bending loss of the FM is < 0.01 dB/m.

5. Conclusion

A novel structure of LMA-PCF with elliptical air hole is proposed and investigated in this paper. On this basis, we propose the idea of using the new parameters of the eccentricity of the ellipse to control the bending losses of the fundamental and first higher order modes. The fiber proposed in this paper can achieve extremely low bending loss under the condition of ensuring large mode area and effective single mode operation. Numerical results show that this structure can achieve

large mode area and effective single-mode operation with low bend loss for the fundamental mode at the wavelength of 1.064 μm. The effective mode area of the fundamental mode is 1228 μm^2 when the bending radius is 15 cm. The bending loss of the fundamental mode is just 9.0038×10^{-4} dB/m, and the loss ratio between the fundamental and high-order modes of the bending loss is larger than 1200 when the bending radius is 15 cm. One of the more significant work of this paper is that the introduction of the new parameters of eccentricity provides a new direction for designing better-performing LMA-PCFs in the future. The fiber structure proposed in this paper has the potential to be applied to compact optical devices, which is of great significance for high-power laser systems and optical amplifiers.

References

[1] J. Nilsson, D. N. Payne, Science **332**(6032), 921 (2011).
[2] D. J. Richardson, J. Nilsson, W. A. Clarkson, J. Opt. Soc. Am. B **27**(11), B63 (2010).
[3] Michalis N.Zervas, C. A. Codemard, IEEE Journal of Selected Topics in Quantum Electronics **20**(5), 219 (2014).
[4] W. Shi, Q. Fang, X. Zhu et al., Applied Optics **53**(28), 6554 (2014).
[5] C. Jauregui, J. Limpert, Andreas Tünnermann, Nature Photonics **7**(11), 861 (2013).
[6] Arlee V. Smith, Jesse J. Smith, Opt. Express **19**(11), 10180 (2011).
[7] Tino Eidam, Christian Wirth, Cesar Jauregui, Fabian Stutzki, Florian Jansen, Hans-Jürgen Otto, Oliver Schmidt, Thomas Schreiber, Jens Limpert, Andreas Tünnermann, Opt. Express **19**(14), 13218 (2011).

[8] Fabian Stutzki, Hans-Jürgen Otto, Florian Jansen, Christian Gaida, Cesar Jauregui, Jens Limpert, Andreas Tünnermann, Opt. Lett. **36**(23), 4572 (2011).

[9] L. Dong, J. Li, X. Peng, Journal of the Optical Society of America B **24**(8), 1689 (2007).

[10] Tsai-wei Wu, Liang Dong, Herbert Winful, Opt. Express **16**(6), 4278 (2008).

[11] A. Liu, D. T. Walton, W. Ji et al., Journal of Lightwave Technology **27**(15), 3010 (2009).

[12] Than Singh Saini, Ajeet Kumar, Ravindra Kumar Sinha, Appl. Opt. **55**(9), 2306 (2016).

[13] Yan Qin, Huajun Yang, Ping Jiang, Fengji Gui, Weinan Caiyang, Biao Cao, Appl. Opt. **57**(14), 3976 (2018).

[14] Shaoshuo Ma et al., Journal of Lightwave Technology **36**(14), 2844 (2018).

[15] S. Ma, T. Ning, L. Pei, J. Li, J. Zheng, X. He et al., Plos One **13**(8), e0203047 (2018).

[16] R. Otupiri, E. K. Akowuah, S. Haxha et al., IEEE Photonics Journal **6**(4), 1 (2014).

[17] Y. Tsuji, M. Koshiba, Journal of Lightwave Technology **18**(4), 618 (2000).

[18] U. Pekel, R. Mittra, IEEE Microwave and Guided Wave Letters **5**(8), 258 (1995).

[19] X. Wang, S. Lou, W. Lu, IEEE Journal of Selected Topics in Quantum Electronics **20**(5), 1(2014).

[20] Ngoc Hai Vu, In-Kag Hwang, Yong-Hee Lee, Opt. Lett. **33**(2), 119 (2008).

[21] Kunimasa Saitoh, Masanori Koshiba, Opt. Express **11**(23), 3100 (2003).

[22] Yukihiro Tsuchida, Kunimasa Saitoh, Masanori Koshiba, Opt. Express **15**(4), 1794 (2007).

[23] Kamyar Rashidi, Seyed Mohammad Mirjalili, Hussein Taleb, Davood Fathi, Journal of Lightwave Technology **36**(23), 5626(2018).

[24] Xiang Chen, Xiongwei Hu, Luyun Yang, Jinggang Peng, Haiqing Li, Nengli Dai, Jinyan Li, Opt. Express **27**(14), 19548 (2019).

[25] She Yu-Lai, Zhou De-Jian, Chen Xiao-Yong, Ni Jia-Ming, Optical Fiber Technology **51**, 101 (2019).

---

*Corresponding author: yanghj@uestc.edu.cn